IEEE Open Journal of the Communications Society

Received XX Month, XXXX; revised XX Month, XXXX; accepted XX Month, XXXX; Date of publication XX Month, XXXX; date of current version 11 January, 2024.

Digital Object Identifier 10.1109/OJCOMS.2024.011100

Predicting Channel Conditions for Adaptive LDPC Coding in a Fading Free-Space Optical Channel

SEMIRA GALIJASEVIC[1] *(Student Member, IEEE)*, JINGCHAO LUO [1], DARIUSH DIVSALAR [2] *(Member, IEEE)* AND RICHARD WESEL[1] *(Member, IEEE)*

[1]Department of Electrical and Computer Engineering, University of California, Los Angeles, CA USA
[2]Jet Propulsion Laboratory, California Institute of Technology, Pasadena, CA, 91109 USA

CORRESPONDING AUTHOR:Semira Galijasevic (e-mail: semiragali@ g.ucla.edu).

This work was supported by CACI under award P000139095 and the National Science Foundation (NSF) under Grant CCF-1955660. Any opinions, findings, and conclusions or recommendations expressed in this material are those of the author(s) and do not necessarily reflect views of NSF. This work was carried out in part at the Jet Propulsion Laboratory, California Institute of Technology, under a contract with NASA.

ABSTRACT Free-space optical (FSO) links are sensitive to channel fading caused by atmospheric turbulence, varying weather conditions, and changes in the distance between the transmitter and receiver. To mitigate FSO fading, this paper applies linear and quadratic prediction to estimate fading channel conditions and dynamically select the appropriate low-density parity check (LDPC) code rate. This adaptivity achieves reliable communication while efficiently utilizing the available channel mutual information. Protograph-based Raptor-like (PBRL) LDPC codes supporting a wide range of rates are designed, facilitating convenient rate switching. When channel state information (CSI) is known without delay, dynamically selecting LDPC code rate appropriately maximizes throughput. This work explores how such prediction behaves as the feedback delay is increased from no delay to a delay of 4 ms for a channel with a coherence time of 10 ms.

INDEX TERMS free space optical channel, LDPC codes, rate adaptive coding

I. INTRODUCTION

A. Background

FREE-SPACE OPTICAL (FSO) communication [1] offers numerous benefits including high date rate, huge licensed free spectrum, high immunity to interference, highly secured links and easy installation [2]–[4]. FSO can be used for communications over distances of several kilometers as well as ultra-long distances such as ground-to-satellite, satellite-to-satellite communications, and interplanetary communications [4].

FSO links are sensitive to channel fading caused by atmospheric turbulence, varying weather conditions, and changes in the distance between the transmitter and receiver. Because of this fading, hybrid communication systems are sometimes deployed where an RF link is used when the FSO link fails [5]–[8]. A novel coding paradigm called "Hybrid Channel Coding" that constructs non-uniform and rate-compatible LDPC codes to achieve the combined channel capacity of parallel FSO and RF channels is introduced in [9]. Simulation analysis in [9] shows that Hybrid Channel Codes can increase the average throughput more than 33% compared to prior systems.

FSO fading has also been mitigated by adaptive parameter selection techniques such as those explored in [9]–[14]. In [10] a rate-adaptive transmission scheme with intensity modulation and direct detection over FSO channel has been studied. The rate-adaptive scheme uses repetition coding and variable silence periods to exploit the potential time-diversity order available in the fading channel [10].

In [11] a scheme to estimate the channel state information (CSI) at the receiver for Raptor and punctured low-density parity check (LDPC) code rate selection is proposed. The receiver sends estimated CSI through a feedback channel to the transmitter where the code rate is selected to accommodate estimated fading channel conditions. The proposed feedback scheme for both coding schemes is evaluated over

short transmission range such that feedback delay is not significant compared to the coherence time of the fading.

Punctured digital video broadcast satellite standard (DVB-S2) LDPC codes combined with channel interleavers are investigated to exploit time diversity in [12]. It is shown that combination of channel coding and bit interleaving technique improves performance in turbulence conditions.

In [13] three different adaptive modulation schemes have been investigated: (i) variable-rate variable-power adaptation, (ii) channel inversion, and (iii) truncated channel inversion schemes. CSI is estimated at the receiver and fed back to the transmitter through RF channel without considering feedback delay. The results show that channel inversion scheme gives similar performance compared to variable-rate variable-power scheme when turbulence is weak, but suffers from significant performance degradation when turbulence is strong.

A rate adaptive scheme using LDPC codes with optimized puncturing is compared to uncoded FSO system and coded FSO system using LDPC codes with random puncturing scheme in [14] . Results show that rate-adaptive FSO systems perform well in realistic FSO systems over different weather conditions. For example, under rainy weather conditions uncoded FSO systems suffer from outages at 87% of the time, while LDPC rate-adaptive systems can successfully utilize 75% to 80% of the signaling rate resulting in a significant increase in throughput. LDPC code rate is selected based on the CSI estimate at the receiver and sent back to the transmitter through an error-free feedback channel. However, in [14] only feedback rate is considered for code rate selection and not the actual feedback channel delay time.

This paper investigates the effect of feedback delay on rate adaptive FSO system with LDPC coding. Rate adaptive LDPC codes provide significant coding gain [15] and efficient encoding and decoding with low hardware complexity [16], [17]. LDPC codes comprise the standard coding technique in Digital Video Broadcasting-Satellite-Second Generation (DVB-S2) [18] and are also utilized by the Optical Communications Terminal (OCT) Standard Version 3.1.0 Developed by the Space Development Agency of the United States Space Force [19].

To mitigate FSO fading, predictive models estimate fading channel conditions to dynamically select LDPC code rate. This achieves reliable communication while efficiently utilizing the available channel mutual information. The three predictive models explored are zero-order prediction, linear prediction and quadratic prediction.

This work examines how these predictive models behave as the feedback delay is increased from no delay to a delay of $4\ ms$ for a channel with a coherence time of $10\ ms$. Protograph-based raptor-like (PBRL) LDPC code with rates $8/9$, $8/10$, ..., $8/80$ are designed using reciprocal channel approximation (RCA) [20] allowing convenient rate switching.

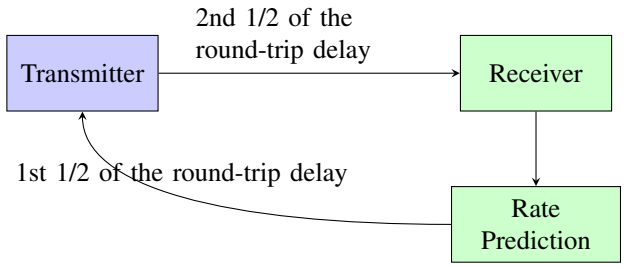

FIGURE 1. Simplified block diagram illustrating round trip of feedback delay time. The first half of the round-trip delay is the duration from when the receiver sends back the predicted rate until the transmitter receives it. The second half of the round-trip delay is the duration for the signal to travel from the transmitter to the receiver.

The fedback delay is the round-trip delay, i.e. the time between the receiver makes the rate prediction and the LDPC code experiences the next fade. A simple block diagram in Fig. 1 illustrates the round trip feedback delay. The first half of the round-trip delay is the time the signal travels back to the transmitter after the receiver predicts the rate and sends it back to the transmitter. The second half of the round-trip delay is the the signal propagation time from the transmitter to the receiver. The receiver experiences the fade exactly one round-trip after it sent the prediction. Note that there is additional small time at the transmitter to compute the codeword after receiving the prediction. However this could be very small or even negligible since the transmission can start even slightly before the rate guidance arrives since the rate determines the total number of symbols and the transmitter will always send at least the number of symbols for the highest rate. Additional time also occurs for the receiver to compute prediction which is negligible compared to the total feedback delay.

The optical channel with a coherence time of $10\ ms$ is meant to model the optical channel of a ow Earth Orbit (LEO) satellite. A typical LEO system usually operates at altitudes ranging from around 160 kilometers (99 miles) to 2,000 kilometers (1,240 miles). The distance corresponding to the specific feedback delay time is calculated as $ct_d/2$, where $c = 3 \times 10^8 m/s$ is speed of light and t_d is round-trip feedback delay time. The round-trip delay times of $2-10\ ms$ correspond to distances of 300 to 1500 kilometers (km). The International Space Station (ISS), for example, has an orbital distance of $400\ km$ while SpaceX's Starlink satellites orbit Earth at a distance of about $550\ km$ above sea level. Project Kuiper satellites will have orbit between 590 and 630 kilometers. The Iridium telecom satellites orbit at about 780 km. Earth observation satellites such as Landsat satellites operate around $705\ km$.

B. Contributions

The main contributions are as follows.

- This paper presents 72 newly designed PBRL LDPC codes supporting a wide range of rates from rate 8/9

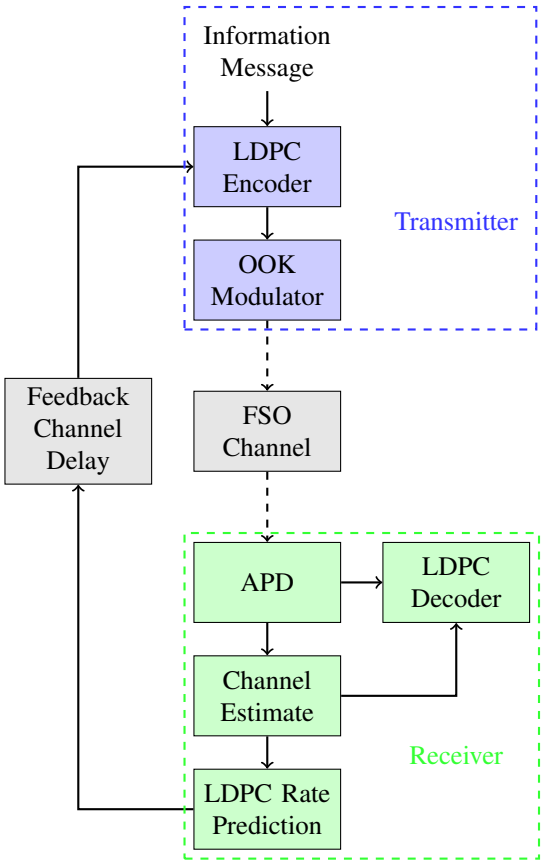

FIGURE 2. **High level system block diagram. The fading channel gain is estimated at the receiver and used to decode the current codeword as well as to predict the future channel gain and corresponding LDPC code rate based on the round-trip delay. The receiver selects the future LDPC code rate such that selected code rate achieves frame error rate (FER) lower than 10^{-6} for predicted channel gain value. The time required for the transmitter to receive a predicted codeword via the feedback channel is equal to half of the round-trip delay.**

to rate 8/80. The rates are designed using RCA [20] to minimize the decoding threshold.

- The analysis shows when CSI is known with no delay, dynamically selecting LDPC code rate based on the CSI maximizes throughput. Such throughput is referred as the zero-delay throughput in this paper.
- This work explores zero-order, linear, and quadratic prediction models to estimate fading channel CSI and dynamically select the LDPC code rate.
- The findings show that the best prediction model depends on the delay. For a channel with a coherence time of 10 ms, linear prediction gives the best throughput performance when feedback delay is less or equal to 2 ms. When feedback delay is equal to 1 or 2 ms, (97.96-100)% of the zero-delay throughput can be achieved.
- Simulations show that quadratic prediction model gives the best performance when feedback delay is 3 or 4 ms, achieving up to 89.92% or 73.67% of the zero-delay throughput, respectively.

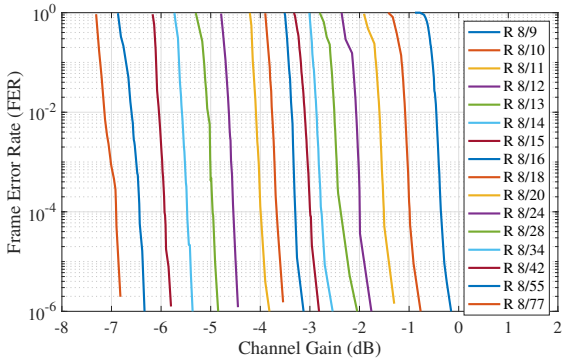

FIGURE 3. **Frame Error Rate (FER) Vs. Channel Gain for LDPC code rates $8/9$ to $8/77$ in descending order from right to left.**

C. Organization

The rest of the paper proceeds as follows. Sec. II introduces the system architecture and FSO channel model. Sec. III presents a theoretical calculation of FER for LDPC codes using the normal approximation. Sec. IV describes LDPC codes designed for a wide range of rates. Sec. V describes three prediction models and presents throughput results achieved by using these predictive models to select the LDPC code rate. Sec. VI concludes this paper.

II. System Model

A. System Architecture

Fig. 2 describes the high level system architecture. The fading channel gain is estimated at the receiver and used to decode the current codeword as well as to predict the future channel gain and corresponding LDPC code rate at a specified future time based on the delay required to transmit the code rate to the transmitter. The receiver selects the future LDPC code rate such that selected code rate achieves frame error rate (FER) lower than 10^{-6} for predicted channel gain value.

Fig. 3 shows FER curves for a subset of the designed LDPC codes as a function of fading channel gain. The highest code rate (8/9) is the rightmost curve. The channel gain thresholds for each LDPC code rate are precomputed and stored in Table 1. The thresholds in Table 1 are calculated by subtracting baseline average power on detector (POD) of $-53.9\ dBm$ from POD for which LDPC code rate achieves FER of 10^{-6}. The selected LDPC code rate is sent back to the transmitter through an error free feedback channel with feedback delay time t_d. The information message is generated at the transmitter side and encoded with LDPC encoder with rate equal to the code rate received via the delayed feedback channel.

B. Fading Channel Model

The channel model (given the fade power ρ) is an asymmetric Gaussian model based on experimentally measured gains in communications performance of a laboratory-based, free-space optical communications system through using

TABLE 1. LDPC codes with channel gain thresholds. Each code rate achieves FER of 10^{-6} for corresponding threshold.

LDPC Code Rate	Threshold [dB]	Margin [dB]
8/9	-0.1522	0.2500
8/10	-0.7672	0.2500
8/11	-1.2802	0.2500
8/12	-1.7596	0.2500
8/13	-2.0459	0.3271
8/14	-2.5409	0.2500
8/15	-2.8154	0.3404
8/16	-3.1276	0.2500
8/18	-3.5267	0.4500
8/20	-3.8154	0.5952
8/24	-4.4457	0.9500
8/28	-4.8492	0.7500
8/34	-5.3644	0.7694
8/42	-5.7939	0.7062
8/55	-6.3336	0.7964
8/77	-6.8036	0.7862

avalanche photodiode detector (APD) at the receiver for signal detection [21]. To compute realizations of temporal fading a sequence of independent and identically distributed (i.i.d.) Gaussian random numbers z_i is filtered by a low-pass filter FIR filter to obtain a band-limited discrete sequence x_i of correlated Gaussian random variables with variance σ_T equal to the Power Scintillation Index. Finally, a memoryless nonlinear block is applied to x_i to obtain the desired log-normal distribution of correlated random variables ρ_i. The autocorrelation function of the log amplitude of scintillation is approximated as

$$R_\rho(\tau) = (\ln(\sigma_T^2 + 1))^2 \exp[-(\tau/\tau_o)^2] \tag{1}$$

, where τ_0 denotes turbulence coherence time [21]. Turbulence coherence time represents a time interval during which the change in fading characteristics of the channel is very small. Fig. 4 shows autocorrelation function for turbulence coherence time of $10\ ms$ as a function of delay τ. As the delay increases the fades are less and less correlated and becoming completely uncorrelated when delay becomes longer than two times the coherence time. The less correlated the fades are, the harder it is to predict future fades.

The modulation scheme used is On-Off keying (OOK) such that each OOK slot contains either the signal (bit 1) or background noise (bit 0) and the baud rate is 2.5 gigasymbols per second. Bit 1 is modulated to μ_1 and bit 0 is modulated to μ_0, where μ_1 is signal current when signal is ON and μ_0 is signal current when signal is OFF. Additive white Gaussian

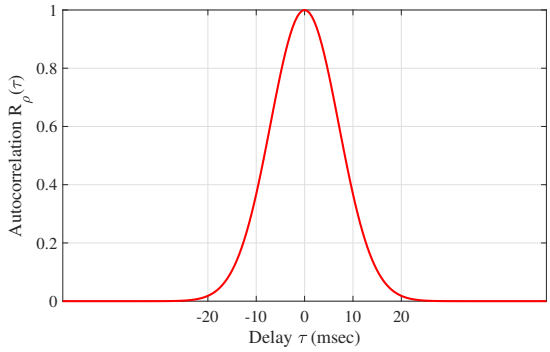

FIGURE 4. Autocorrelation function $R_\rho(\tau)$ for turbulence coherence time of $\tau_0 = 10\ ms$.

noise (AWGN) is added to the signal so that the observations for both signal (ON) for bit 1 and signal (OFF) for bit 0 are modeled using Gaussian distributions $\mathcal{N} \sim (\mu_1, \sigma_1^2)$ and $\mathcal{N} \sim (\mu_0, \sigma_0^2)$. Here σ_1 and σ_0 denote total noise when signal is ON and OFF respectively. Thus, the log-likelihood ratio (LLR) used by LDPC decoder is given by:

$$LLR = \frac{1}{2} \ln \frac{\sigma_0^2}{\sigma_1^2} + \frac{(y-\mu_0)^2}{2\sigma_0^2} - \frac{(y-\mu_1)^2}{2\sigma_1^2} \tag{2}$$

Equations (3)–(11) describe the calculations of μ_1, σ_1, μ_0 and σ_0. The meanings and values of variables and constants used in the equations are given in Table 2.

$$\mu_1 = res\ apd_1\ 10^{\frac{pod_1}{10}-3} \tag{3}$$

$$\mu_0 = res\ apd_0\ 10^{\frac{pod_0}{10}-3} \tag{4}$$

$$ex_1 = k_{eff}\ apdg_1 + (1-k_{eff})\left(2 - \frac{1}{apdg_1}\right) \tag{5}$$

$$ex_0 = k_eff\ apdg_0 + (1-k_{eff})\left(2 - \frac{1}{apdg_0}\right) \tag{6}$$

$$sigshot_1 = (2\ q\ \mu_1\ apdg_1\ ex_1)^{\frac{1}{2}} \tag{7}$$

$$sigshot_0 = (2\ q\ \mu_0\ apdg_0\ ex_0)^{\frac{1}{2}} \tag{8}$$

$$darkshot_i = (2\ q\ ex_i\ (apdg_i)^2\ I_{dark})^{\frac{1}{2}}, \quad i = 0, 1 \tag{9}$$

$$\sigma_1 = \left(B_{ef}\ (sigshot_1^2 + darkshot_1^2 + D_{TIA}^2)\right)^{\frac{1}{2}} \tag{10}$$

$$\sigma_0 = \left(B_{ef}\ (sigshot_0^2 + darkshot_0^2 + D_{TIA}^2)\right)^{\frac{1}{2}} \tag{11}$$

Since the channel fading is changing slowly with respect to the codeword length, simulations are performed over a block fading model described in [8] and [22]. The simulation model in [8] is used to generate fading channel gain samples for turbulence coherence time of 10 ms.

Note that for the given baud rate of 2.5 gigasymbols per second, the time occupancy of each codeword ranges from 3.6864 micro-seconds (μs) for the highest code rate $(8/9)$ to 31.539 μs for the lowest code rate $(8/77)$, which is relatively small compared to the turbulence coherence time. The fading model generates one fade value for every 1024 bits which means that different sections of a codeword will experience a different fade. However, since the turbulence coherence time

TABLE 2. Constants and variables used to calculate signal current μ_1 and total noise σ_1 when signal is ON, and signal current μ_0 and total noise σ_0 when signal is OFF.

Symbol	Quantity	Value	Unit
q	electron charge	1.6×10^{-19}	C
$apdg_1$	APD gain when bit 1 is sent	15	dB
$apdg_0$	APD gain when bit 0 is sent	15	dB
res	responsivity	0.9	A/W
B_{ef}	electronic filter bandwidth	120	MHz
k_{ef}	impact coefficient	0.2	
I_{dark}	dark current	2.1×10^{-8}	A
D_{TIA}	Transimpedance Amplifier (TIA) input noise current density	2×10^{-12}	$\frac{A}{\sqrt{Hz}}$
POD_{ave}	average power on detector	$[-58, -54]$	dBm
r_{ext}	extinction ratio	11	dB
POD_1	power on detector when bit 1 is sent	$pod_{ave}+\frac{r_{ext}}{2}$	dBm
POD_0	power on detector when bit 0 is sent	$pod_{ave}-\frac{r_{ext}}{2}$	dBm

is much longer than the time occupancy of a codeword these differences are negligible.

III. Theoretical Analysis

For FSO On-Off Keying (OOK) with equal likely transmission of bit 1 and 0, consider the following channel model when bit 1 (On) or bit 0 (Off) is transmitted:

$$y = \mu_i + \sigma_i n, \quad i = 0 \text{ or } 1 \tag{12}$$

where n is zero mean, unit variance normal, then given the fade power, y is a Gaussian random variable with probability density function $p_i(y)$ which is normal distributed $N(\mu_i, \sigma_i^2)$.

When bit 1 is transmitted the channel information density is

$$i_1(y) = 1 - \log_2\left(1 + \frac{\sigma_1}{\sigma_0} e^{-\frac{1}{2\sigma_0^2}(y-\mu_0)^2 + \frac{1}{2\sigma_1^2}(y-\mu_1)^2}\right) \tag{13}$$

and its nth moment after change of variable is

$$m_n(i_1) = \int_{-\infty}^{\infty} p_1(y) i_1^n(y) dy = \int_{-\infty}^{\infty} \frac{1}{\sqrt{2\pi}} e^{-\frac{z^2}{2}} i_1^n(z) dz \tag{14}$$

where

$$i_1(z) = 1 - \log_2\left(1 + \frac{\sigma_1}{\sigma_0} e^{-\frac{1}{2\sigma_0^2}(\sigma_1 z + \mu_1 - \mu_0)^2 + \frac{1}{2}z^2}\right) \tag{15}$$

When bit 0 is transmitted the channel information density is

$$i_0(y) = 1 - \log_2\left(1 + \frac{\sigma_0}{\sigma_1} e^{-\frac{1}{2\sigma_1^2}(y-\mu_1)^2 + \frac{1}{2\sigma_0^2}(y-\mu_0)^2}\right) \tag{16}$$

and its nth moment after change of variable is

$$m_n(i_0) = \int_{-\infty}^{\infty} p_0(y) i_0^n(y) dy = \int_{-\infty}^{\infty} \frac{1}{\sqrt{2\pi}} e^{-\frac{z^2}{2}} i_0^n(z) dz \tag{17}$$

where

$$i_0(z) = 1 - \log_2\left(1 + \frac{\sigma_0}{\sigma_1} e^{-\frac{1}{2\sigma_1^2}(\sigma_0 z + \mu_0 - \mu_1)^2 + \frac{1}{2}z^2}\right) \tag{18}$$

The average of channel information density with equal probable channel inputs is

$$C = \frac{1}{2}[m_1(i_1) + m_1(i_0)] \tag{19}$$

and the channel dispersion with equal probable channel inputs is

$$V = \frac{1}{2}[m_2(i_1) + m_2(i_0)] - C^2 \tag{20}$$

Both $C(POD)$ and $V(POD)$ are functions of the average received power POD at APD.

Using the Normal Approximation by Polyanskiy [23], the maximal achievable rate can be approximated by

$$R^*(n, FER) = C - \sqrt{\frac{V}{n}} Q^{-1}(FER) + O(\frac{\log_2 n}{n}) \tag{21}$$

where $Q^{-1}(.)$ denotes inverse of the Gaussian Q-function which is

$$Q(x) = \int_x^{\infty} \frac{1}{\sqrt{2\pi}} e^{-\frac{1}{2}y^2} dy \tag{22}$$

then the FER can be calculated as

$$FER(POD) = Q\left(\frac{C(POD) - R + \log_2(n)/2n}{\sqrt{V(POD)/n}}\right) \tag{23}$$

where R represent the code rate and $n = k/R$ is codeword block length, k is the message block length, and $O(\frac{\log_2 n}{n}) \approx \log_2(n)/2n$. However for $k = 8192$ the same FERs have been obtained for all code rates by ignoring the $O(.)$ term. As an example consider a laser with extinction ratio of 11 dB, and an APD detector, such that observations can be expressed as, $\mu_1 = \alpha_1 POD$, $\mu_0 = \alpha_0 POD$, $\sigma_1^2 = \beta_1 POD + \gamma_1$, and $\sigma_0^2 = \beta_0 POD + \gamma_0$, where $\alpha_1 = 47.7$, $\alpha_0 = 3.8$, $\beta_1 = 1.25 \times 10^{-7}$, $\beta_0 = 9.9 \times 10^{-9}$ and $\gamma_1 = \gamma_0 = 1.3 \times 10^{-15}$. In this paper block fading is considered where the fade power ρ is constant over duration of codeword. This assumption is valid when the coherence time of fading is larger than duration of codeword. The fading power is normalized such that $E\{\rho\} = 1$.

In the fading channel model then POD is replaced with ρPOD. For the atmospheric fading the Power Scintillation Index PSI=10 is assumed. The FERs using normal approximation for rates 8/9 to 8/77 as in Table 1 are plotted in Fig. 5. The thresholds in Table 1 are computed based on reference point average POD of -53.9 dBm. and compared with thresholds using normal approximation. This comparison

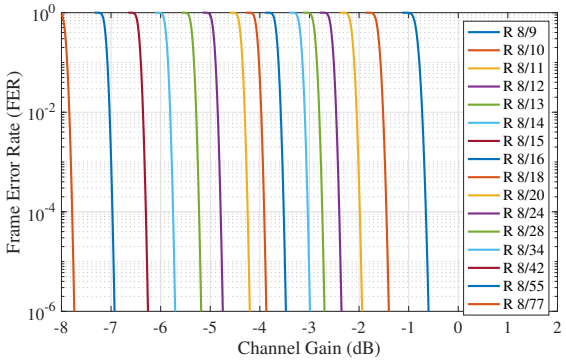

FIGURE 5. Frame Error Rate (FER) vs Channel Gain using Normal Approximation (NA).

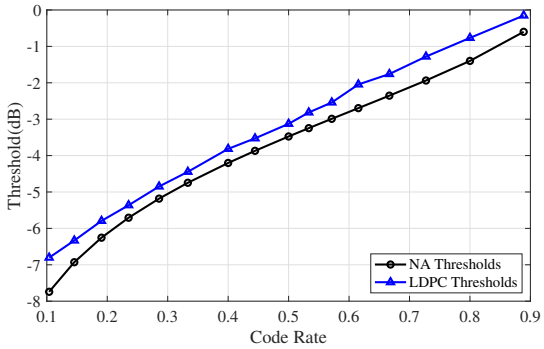

FIGURE 6. The thresholds in Table 1 are compared with thresholds using normal approximation (NA).

is shown in Fig. 6. The close proximity of the thresholds indicates the excellent LDPC code performance.

One way to see how adaptively adjusting the rate can improve performance for slow fading is to compute the FER that a fixed-rate system would provide. To compute the theoretical performance of a fixed -rate scheme in slow fading without feedback, we integrate the product of the density $f(\rho)$ of ρ from [22] and the FER from (23) (denote that by $F(POD)$) with POD replaced with ρPOD for a fixed-rate random code, as shown below:

$$FER = \int_{\rho=0}^{\infty} F(\rho POD) f(\rho) d\rho \,. \tag{24}$$

assuming that $f(\rho)$ the pdf of fade power ρ is normalized such that $E\{\rho\} = 1$. Such a computation reveals that the FER performance for the fixed-rate scheme incurs a huge performance loss.

IV. Low-Rate Protograph-based LDPC Codes Design

This paper uses the PBRL [20] approach to design LDPC codes with information blocklength $k = 8192$ and parity check matrix $\mathbf{H}$ described by Eqn. 25 for wide range of rates. Let n_1 represent the number of variable nodes in $\mathbf{H_{HRC}}$ and m_1 number of rows in $\mathbf{H_{IRC}}$ matrix. In Eqn. 25 submatrix $\mathbf{H}_{\text{HRC}} \in \mathbb{F}_2^{(n_1-k)\times n_1}$ represents highest-code rate (HRC) and submatrix $\mathbf{H}_{\text{IRC}} \in \mathbb{F}_2^{m_1\times n_1}$ represents an incremental redundancy code (IRC). PBRL LDPC code supports rates from $\frac{k}{n_1-n_p}$ to $\frac{k}{n_1+m_1-n_p}$ by puncturing degree-1 variable nodes associated with identity matrix in Eqn. 25, where n_p represents number of punctured nodes. This work presents designed H_{IRC} to support the lowest code rate of $1/10$. Thus, $m_1 = 72704$ and $n_1 = 9216$.

$$\mathbf{H} = \begin{bmatrix} \mathbf{H}_{\text{HRC}} & \mathbf{0} \\ \mathbf{H}_{\text{IRC}} & \mathbf{I} \end{bmatrix}, \tag{25}$$

$\mathbf{H}_{\text{HRC}}$ is obtained from its proto-matrix. $\mathbf{H}_{\text{HRC}}$ proto-matrix in Eqn. 26 is adopted from [8].

$$\mathbf{H}_{\text{HRC}} = [\ 4 \quad 4 \quad 4 \quad 4 \quad 4 \quad 3 \quad 3 \quad 3 \quad 3\ ] \tag{26}$$

Unlike LDPC codes that start with a designed lowest rate code and increase the rate by randomly puncturing variable nodes hoping to not degrade performance, PBRL design starts with well designed highest rate code and obtains the lower code rates by carefully selecting the rows of $\mathbf{H}_{\text{IRC}}$. The design is done in two steps.

In the first step, the proto-matrix $\mathbf{H}_{\text{IRC}}$ [24] is designed line by line in a greedy fashion by minimizing decoding threshold of newly constructed protograph matrix computed using the reciprocal channel approximation (RCA) algorithm [20]. The decoding threshold of a protograph matrix refers to the minimum channel noise that supports reliable iterative decoding of LDPC codes with infinite code length built from the protograph. The fully designed protograph matrix of $\mathbf{H}$ for rate $1/10$ consists of 72 rows (check nodes) and 80 columns (variable nodes).

The designed protograph matrix for lowest code rate of $1/10$ is lifted using approximate-cycle extrinsic-message-degree (ACE) progressive-edge-growth (PEG) algorithm [25] to replace each element in protograph matrix with circulant matrices and obtain parity check matrix $\mathbf{H}$ with longer block-length. The ACE-PEG algorithm with parameters of $d_{ACE} = 6$ and $\eta = 7$ are selected to ensure that all the cycles in the lifted parity check matrix whose length is 12 or less have ACE values of at least 7.

The lifting process consists of two steps. In the first step lifting number is 4 to remove parallel edges in protograph matrix. In the second step lifting number is 256 which gives a parity check matrix with information blocklength of 8192 bits. Fig. 3 shows FER as a function of fading channel gain for a subset of the designed LDPC code rates. Fig. 6 compares performance between designed LDPC codes and normal approximation for FER of 10^{-6}.

V. LDPC Rate Selection To Maximize Throughput

This section presents different predictive models for selecting LDPC code rate based on the knowledge of channel gain and feedback time delays. The fading channel gains are estimated at the receiver and used to predict a future channel gain considering the delay required to transmit the signal from the receiver back to the transmitter. The receiver uses predicted channel gain value to select LDPC code rate that achieves

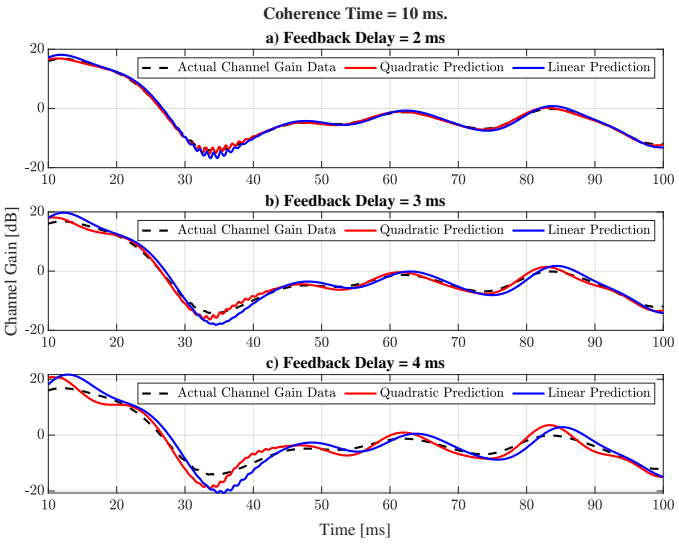

FIGURE 7. Comparison of channel gain values for quadratic and linear prediction with respect to the actual fading channel gain values when coherence time is $10\ ms$ and feedback delay ranges from $2\ ms$ to $4\ ms$.

FER lower than 10^{-6} for predicted channel gain. For the purpose of analysis, out of 72 designed code rates a subset of 16 code rates with approximate threshold differences of 0.5 dB is selected. The channel gain thresholds for which each LDPC code rate decodes a codeword with FER of 10^{-6} are given in Table 1.

A. Instantaneous Channel State Information

As a baseline for comparison, we consider the case where the feedback delay is zero and current channel state is known. The LDPC code rate is selected to maximize throughput, i.e. the code rate selected is the highest code rate that achieves FER below 10^{-6} for the current known channel state. Actual channel gain data is represented with dashed black curve in Fig. 7. Throughput achieved when the receiver knows the CSI with no delay is referred as zero-delay throughput and it is used as a reference to evaluate the performance of prediction models when feedback delay is not zero.

B. Delayed Channel State Information

Now we consider the practical scenario where the feedback delay is not zero.

1) Zero-Order Prediction

The zero-order prediction model predicts fading channel gain value in the future to be the same as the current channel estimate at the receiver. Let fading channel gain value estimated at the receiver at time t_k be c_k and let t_d denote the feedback channel delay time. The estimated channel gain value c_{k+d} at time $(t_k + t_d)$ is the same as c_k.

2) Linear Prediction

Let $\mathbf{c} = [c_1, c_2, ..., c_n]$, $c_i \in \mathbb{R}$ represent fading channel gain values estimated by the receiver. Let $\mathbf{t} = [t_1, t_2, ..., t_n]$, $t_i \in \mathbb{R}$ represent time instances that correspond to the received fading channel gain values in $\mathbf{c}$. In order to make a prediction of channel gain in the future the estimated channel gain data is used to fit a polynomial of a form :

$$p(t) = x_1 + x_2\mathbf{t} + ... + x_m\mathbf{t}^{m-1} \tag{27}$$

For each coefficient x a vector of errors $\mathbf{e} = [p(t_1) - c_1, p(t_2) - c_2, ..., p(t_n) - c_n]$ is formed. As described in [26], to find a polynomial that minimizes the norm of the error vector $\mathbf{e}$ following norm approximation problem is solved:

$$\min_{\mathbf{x}} ||\mathbf{e}|| = ||\mathbf{Ax} - \mathbf{c}|| \tag{28}$$

where $A_{ij} = t_i^{j-1}$, $i = 1, 2, ..., n$, $j = 1, 2, ..., m$. Once a solution vector $\mathbf{x}$ is obtained, a predicted channel gain at some time instance t_k is calculated by plugging t_k into Eqn. 27. MATLAB function *polyfit* is used to solve problem in Eqn. 28. Linear prediction model fits a line ($m = 2$) using estimated past CSI to predict future CSI.

In this paper the receiver starts prediction calculations upon the receipt of the first codeword which code rate is chosen to be $8/16$ for simulation purposes. Since each fade represents 1024 bits, the receiver will estimate 16 channel gain values. This is the smallest number of samples used to fit a polynomial to predict a future channel gain. As more samples arrive at the receiver each new prediction is modeled using more samples. The maximum number of channel gain samples used in linear prediction model is equivalent to the half of the feedback delay.

3) Quadratic Prediction

Quadratic prediction model fits polynomial in Eqn. 27 for $m = 3$ using past estimated CSI to predict future CSI for LDPC code rate selection. The maximum number of channel gain samples used in quadratic prediction is equal to the two times the feedback delay when delay is $1\ ms$ and simply the feedback delay in all other cases. We observed that adding a small margin to the original thresholds determined in Table I improved our FER performance. These margin values are included in Table I.

Fig. 7 compares channel gain data obtained using linear and quadratic prediction models when feedback delay increases from $2\ ms$ to $4\ ms$ with actual channel gain data over the time interval of $10\ ms$ to $100\ ms$.

Fig. 8 shows actual and predicted channel gain values for zero order, linear order and quadratic prediction when turbulence coherence time is $10\ ms$ and feedback channel delay is $2\ ms$. The maximum number of channel gain values used for fitting linear model is equal to half of delay ($1\ ms$) of samples. The maximum number of samples used for fitting quadratic model is equal to delay ($2\ ms$) of samples.

Fig. 9 shows the percentage of zero-delay throughput achieved using each prediction model as a function of

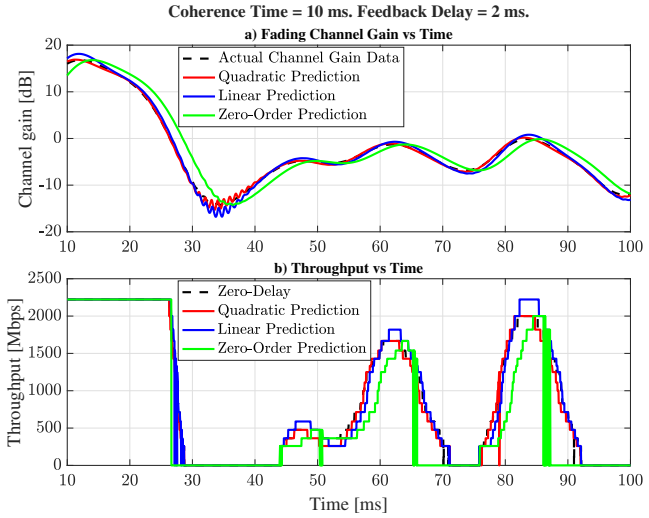

FIGURE 8. a) Actual and predicted channel gain values vs. time. The maximum number of samples used for fitting linear model is equal to half of delay ($1\ ms$) worth of samples. The maximum number of samples used for fitting quadratic model is equal to delay ($2\ ms$) worth of samples. b) Throughput vs. time obtained using zero-delay, zero-order, linear and quadratic prediction models for fading channel conditions in a). Turbulence coherence time is $10\ ms$, feedback delay is $2\ ms$ and baud rate is 2.5 Gbps.

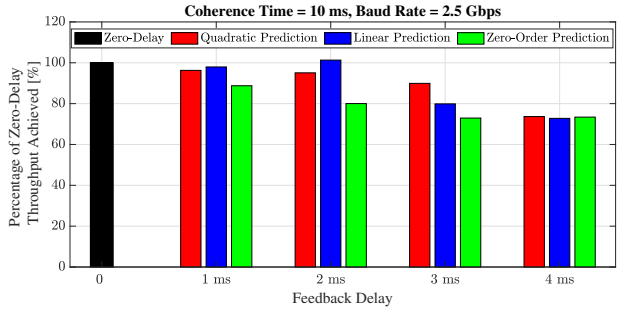

FIGURE 9. Percentage of zero-delay throughput achieved using prediction models as a function of feedback delay when coherence time is $10\ ms$ and feedback delay ranges from $1\ ms$ to $4\ ms$. Linear prediction model gives the best performance for shorter feedback delay times ($1\ ms$ and $2\ ms$). Quadratic prediction model gives the best performance for longer feedback delay timces ($3\ ms$ and $4\ ms$).

feedback delay when coherence time is $10\ ms$. The feedback delay ranges from $1\ ms$ to $4\ ms$. The linear prediction model gives the best performance for shorter delay times achieving 97.96% and 101.3% of zero-delay throughput for feedback delays of $1\ ms$ and $2\ ms$ respectively. Intuitively, this is expected since the fade changes in Fig. 8 that occur within $2\ ms$ are not severe to cause significant outliers when fitting a line to the CSI data. Note that 101.3% is due to the linear prediction model occasionally overestimating channel gain values at the peaks where the values change direction from increasing to decreasing. At these peaks, the model sometimes successfully selects a higher code rate compared to zero-delay model. Since we are considering thresholds below FER of 10^{-6}, the selected code rate might still have a high chance of success which happened in the simulation for a $2\ ms$ feedback delay. As feedback delay increases, the changes between fades are more severe resulting in significant outliers within the CSI data when fitting a linear model. Thus, to minimize the norm of the error vector when feedback delay is greater than $2\ ms$, a higher order polynomial fitting model such as quadratic will fit the data better as confirmed by simulation results in Fig. 9. The quadratic prediction model gives the best performance for longer feedback delay times achieving 89.92% and 73.67% of zero-delay throughput for feedback delays of $3\ ms$ and $4\ ms$ respectively.

VI. Conclusions

For an FSO fading channel when CSI is known with no delay, the throughput is maximized by selecting the rate accordingly. This paper presents three prediction models to mitigate the FSO fading when feedback delay is not zero. For a fading optical channel with a coherence time of 10 ms, the linear prediction model performs best for feedback delays of $1\ ms$ and $2\ ms$. The quadratic prediction model performs best for feedback delays of $3\ ms$ and $4\ ms$. Simulation results suggest that these prediction models can achieve 100% to 73.67% of the zero-delay throughput as feedback delay ranges from $1\ ms$ to $4\ ms$. Thus, for a LEO satellite such as the ISS with an orbital distance of 400 km, quadratic prediction will perform best when the ISS first comes into view, then linear prediction will be best as it flies overhead, with quadratic prediction again being preferred as it moves towards the opposite horizon.

REFERENCES

[1] M. Leba, S. Riurean, and A. Lonica, "Lifi — the path to a new way of communication," in *2017 12th Iberian Conference on Information Systems and Technologies (CISTI)*, 2017, pp. 1–6.

[2] M. A. Khalighi and M. Uysal, "Survey on free space optical communication: A communication theory perspective," *IEEE Communications Surveys & Tutorials*, vol. 16, no. 4, pp. 2231–2258, 2014.

[3] H. T. T. Pham, N. T. Dang, L. T. Vu, and H. T. Bui, "A survey of performance improvement methods for free-space optical communication systems," in *2014 International Conference on Advanced Technologies for Communications (ATC 2014)*, 2014, pp. 770–775.

[4] M. Uysal and H. Nouri, "Optical wireless communications — an emerging technology," in *2014 16th International Conference on Transparent Optical Networks (ICTON)*, 2014, pp. 1–7.

[5] B. Bag, A. Das, I. S. Ansari, A. Prokeš, C. Bose, and A. Chandra, "Performance analysis of hybrid FSO systems using FSO/RF-FSO link adaptation," *IEEE Photonics Journal*, vol. 10, no. 3, pp. 1–17, 2018.

[6] M. N. Khan, S. O. Gilani, M. Jamil, A. Rafay, Q. Awais, B. A. Khawaja, M. Uzair, and A. W. Malik, "Maximizing throughput of hybrid FSO-RF communication system: An algorithm," *IEEE Access*, vol. 6, pp. 30 039–30 048, 2018.

[7] M. M. Abadi, Z. Ghassemlooy, S. Zvanovec, M. R. Bhatnagar, and Y. Wu, "Hard switching in hybrid FSO/RF link: Investigating data rate and link availability," in *2017 IEEE International Conference on Communications Workshops (ICC Workshops)*, 2017, pp. 463–468.

[8] J. Nguyen, E. M. Liang, L. Wang, R. D. Wesel, T. Drullinger, and T. Chauvin, "Comparison of integrated and independent RF/FSO transceivers on a fading optical channel," in *2020 54th Asilomar Conference on Signals, Systems, and Computers*, 2020, pp. 699–701.

[9] A. Eslami, S. Vangala, and H. Pishro-Nik, "Hybrid channel codes for efficient FSO/RF communication systems," *IEEE Transactions on Communications*, vol. 58, no. 10, pp. 2926–2938, 2010.

[10] A. García-Zambrana, C. Castillo-Vázquez, and B. Castillo-Vázquez, "Rate-adaptive FSO links over atmospheric turbulence channels by jointly using repetition coding and silence periods," *Opt. Express*, vol. 18, no. 24, pp. 25 422–25 440, Nov 2010. [Online]. Available: https://opg.optica.org/oe/abstract.cfm?URI=oe-18-24-25422
[11] J. A. Anguita, M. A. Neifeld, B. Hildner, and B. Vasic, "Rateless coding on experimental temporally correlated FSO channels," *Journal of Lightwave Technology*, vol. 28, no. 7, pp. 990–1002, 2010.
[12] M. Czaputa, T. Javornik, E. Leitgeb, G. Kandus, and Z. Ghassemlooy, "Investigation of punctured LDPC codes and time-diversity on free-space optical links," in *Proceedings of the 11th International Conference on Telecommunications*, 2011, pp. 359–362.
[13] I. B. Djordjevic, "Adaptive modulation and coding for free-space optical channels," *Journal of Optical Communications and Networking*, vol. 2, no. 5, pp. 221–229, 2010.
[14] L. Liu, M. Safari, and S. Hranilovic, "Rate-adaptive FSO communication via rate-compatible punctured LDPC codes," in *2013 IEEE International Conference on Communications (ICC)*, 2013, pp. 3948–3952.
[15] T. Mizuochi, "Recent progress in forward error correction and its interplay with transmission impairments," *IEEE Journal of Selected Topics in Quantum Electronics*, vol. 12, no. 4, pp. 544–554, 2006.
[16] B. Vasic and O. Milenkovic, "Combinatorial constructions of low-density parity-check codes for iterative decoding," *IEEE Transactions on Information Theory*, vol. 50, no. 6, pp. 1156–1176, 2004.
[17] B. Vasic and I. B. Djordjevic, "Iteratively decodable block codes for long haul optical transmission systems," *Journal of Optical Communications*, vol. 23, no. 5, pp. 182–186, 2002. [Online]. Available: https://doi.org/10.1515/JOC.2002.23.5.182
[18] ETSI EN 302 307, "Digital video broadcasting (DVB); second generation framing structure, channel coding and modulation systems for broadcasting, interactive services, news gathering and other broadband satellite applications (DVB-S2)."
[19] Space Development Agency, "Optical communications terminal (OCT) standard version 3.1.0."
[20] T.-Y. Chen, K. Vakilinia, D. Divsalar, and R. D. Wesel, "Protograph-based raptor-like LDPC codes," *IEEE Transactions on Communications*, vol. 63, no. 5, pp. 1522–1532, 2015.
[21] M. W. Wright, M. Srinivasan, and K. Wilson, "Improved Optical Communications Performance Using Adaptive Optics with an Avalanche Photodiode Detector," *Interplanetary Network Progress Report*, vol. 42-161, pp. 1–13, May 2005.
[22] Z. Kolka, V. Biolková, and D. Biolek, "Channel model for monte-carlo simulation of data transmission on terrestrial FSO paths," 2014. [Online]. Available: https://api.semanticscholar.org/CorpusID:53313155
[23] Y. Polyanskiy, H. V. Poor, and S. Verdu, "Channel coding rate in the finite blocklength regime," *IEEE Transactions on Information Theory*, vol. 56, no. 5, pp. 2307–2359, 2010.
[24] "LDPC HRC and IRC proto-matrices for FSO Channel." [Online]. Available: http://www.seas.ucla.edu/csl/publications/published-codes-and-design-tools
[25] T. Tian, C. Jones, J. Villasenor, and R. Wesel, "Selective avoidance of cycles in irregular LDPC code construction," *IEEE Transactions on Communications*, vol. 52, no. 8, pp. 1242–1247, 2004.
[26] S. Boyd and L. Vandenberghe, *Convex Optimization*. Cambridge University Press, 2004, ch. 6.5.3.

FIRST A. AUTHOR (Fellow, IEEE) and all authors may include biographies. Biographies are often not included in conference-related papers. This author became a Member (M) of IEEE in 1976, a Senior Member (SM) in 1981, and a Fellow (F) in 1987. The first paragraph may contain a place and/or date of birth (list place, then date). Next, the author's educational background is listed. The degrees should be listed with type of degree in what field, which institution, city, state, and country, and year the degree was earned. The author's major field of study should be lower-cased.

The second paragraph uses the pronoun of the person (he or she) and not the author's last name. It lists military and work experience, including summer and fellowship jobs. Job titles are capitalized. The current job must have a location; previous positions may be listed without one. Information concerning previous publications may be included. Try not to list more than three books or published articles. The format for listing publishers of a book within the biography is: title of book (publisher name, year) similar to a reference. Current and previous research interests end the paragraph. The third paragraph begins with the author's title and last name (e.g., Dr. Smith, Prof. Jones, Mr. Kajor, Ms. Hunter). List any memberships in professional societies other than the IEEE. Finally, list any awards and work for IEEE committees and publications. If a photograph is provided, it should be of good quality, and professional-looking. Following are two examples of an author's biography.

SECOND B. AUTHOR was born in Greenwich Village, New York, NY, USA in 1977. He received the B.S. and M.S. degrees in aerospace engineering from the University of Virginia, Charlottesville, in 2001 and the Ph.D. degree in mechanical engineering from Drexel University, Philadelphia, PA, in 2008.

From 2001 to 2004, he was a Research Assistant with the Princeton Plasma Physics Laboratory. Since 2009, he has been an Assistant Professor with the Mechanical Engineering Department, Texas A&M University, College Station. He is the author of three books, more than 150 articles, and more than 70 inventions. His research interests include high-pressure and high-density nonthermal plasma discharge processes and applications, microscale plasma discharges, discharges in liquids, spectroscopic diagnostics, plasma propulsion, and innovation plasma applications. He is an Associate Editor of the journal *Earth, Moon, Planets*, and holds two patents.

Dr. Author was a recipient of the International Association of Geomagnetism and Aeronomy Young Scientist Award for Excellence in 2008, and the IEEE Electromagnetic Compatibility Society Best Symposium Paper Award in 2011.

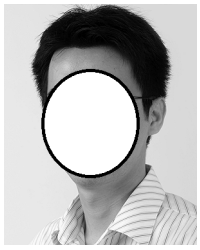

THIRD C. AUTHOR, JR. (Member, IEEE) received the B.S. degree in mechanical engineering from National Chung Cheng University, Chiayi, Taiwan, in 2004 and the M.S. degree in mechanical engineering from National Tsing Hua University, Hsinchu, Taiwan, in 2006. He is currently pursuing the Ph.D. degree in mechanical engineering at Texas A&M University, College Station, TX, USA.

From 2008 to 2009, he was a Research Assistant with the Institute of Physics, Academia Sinica, Tapei, Taiwan. His research interest includes the development of surface processing and biological/medical treatment techniques using nonthermal atmospheric pressure plasmas, fundamental study of plasma sources, and fabrication of micro- or nanostructured surfaces.

Mr. Author's awards and honors include the Frew Fellowship (Australian Academy of Science), the I. I. Rabi Prize (APS), the European Frequency and Time Forum Award, the Carl Zeiss Research Award, the William F. Meggers Award and the Adolph Lomb Medal (OSA).